Modification of Magnetic Properties of Pt/Co/Pt Films by Ga^+ Ion Irradiation: Focused versus Uniform Irradiation

I. Sveklo[a,*], P. Mazalski[a,b], J. Jaworowicz[a,c], J.-P. Jamet[c], N. Vernier[c], A. Mougin[c], J. Ferré[c], M. Kisielewski[a], V. Zablotskii[a,d], E. Bourhis[e], J. Gierak[e], K. Postava[f], J. Fassbender[g], J. Kanak[h] and A. Maziewski[a]

[a]Faculty of Physics, University of Białystok, K. Ciołkowskiego 1L, 15-245 Białystok, Poland
[b]Jerzy Haber Institute of Catalysis and Surface Chemistry, Polish Academy of Sciences, Niezapominajek 8, 30-239 Krakow, Poland
[c]Laboratoire de Physique des Solides, Université Paris-Sud, CNRS UMR 8502, F-91405 Orsay Cedex, France
[d]Institute of Physics CAS, Prague, 18221, Czech Republic
[e]Laboratoire de Photonique et de Nanostructures, CNRS UPR 20, Marcoussis, F-91460, France
[f]IT4Innovations and Nanotechnology Centre, VSB-Technical University of Ostrava, 17 Listopadu 15, 708 33 Ostrava-Poruba, Czech Republic
[g]Helmoltz-Zentrum Dresden-Rossendorf, 01328 Dresden, Germany
[h]Department of Electronics, AGH University of Science and Technology, al. A. Mickiewicza 30, 30-059 Krakow, Poland

(Received July 4, 2017; in final form February 16, 2018)

30 keV Ga^+ irradiation-induced changes of magnetic and magneto-optical properties of sputtered Pt/Co/Pt ultrathin trilayers films have been studied as a function of the ion fluence. Out-of-plane magnetic anisotropy states with enhanced magneto-optical effects were evidenced for specific values of cobalt thickness and irradiation fluence. Results obtained after uniform or quasi-uniform focused ion beam irradiation on either out-of-plane or in-plane magnetized sputtered pristine trilayers are compared. Similar irradiation-induced magnetic changes are evidenced in quasi-uniformly focused ion beam or uniformly irradiated films, grown either by sputtering or molecular beam epitaxy. We discuss on plausible common mechanisms underlying the observed effects.

DOI: 10.12693/APhysPolA.133.1215

PACS/topics: ultrathin films, ion irradiation, magnetic hysteresis, magnetic anisotropy, magneto-optic Kerr effect

1. Introduction

More than ten years ago, it has been demonstrated that magnetic thin film properties may be modified and even well controlled by He^+ ion irradiation under moderate fluences [1–4]. As a consequence, patterning of nanoelements can be successfully achieved by uniform He^+ ion irradiation through masks designed by electron beam lithography [1, 3]. Pt/Co ultrathin films or multilayers with perpendicular magnetic anisotropy (PMA) are the most investigated systems so far to evaluate irradiation-induced changes of magnetism [5]. For irradiation by light He^+ ions, structural and magnetic changes arise only from ballistic ion collisions that favor disordering and intermixing at Co–Pt interfaces. Generally, ion-bombardment-driven modifications of Co films can be considered for two ranges of cobalt thickness d_{Co}, namely smaller or larger than d_{SRT} — the critical Co thickness at the out-of-plane to in-plane spin reorientation transition (SRT) [6]. Considering Pt/Co(d_{Co})/Pt pristine films with PMA ($d_{Co} < d_{SRT}$), irradiation by He^+ ions reduces the magnetic interface anisotropy contribution [1, 3], the coercivity [1, 7] and the Curie temperature [7, 8] to finally trigger a SRT [9, 10]. From another hand, in chemically disordered FePt films, it has been shown that He^+ ion irradiation significantly reduces the annealing temperature required for $L1_0$ alloy ordering [2, 11] and reinforces the magnetic anisotropy volume contribution.

In the same Co/Pt film structures with PMA, irradiation by heavy ions strengthens the ion mixing process [2, 12] which differs significantly from that induced by light He^+ ions. Thus, collision cascades between the incoming Ga^+ ions and Pt or Co atoms are highly favored, enhancing drastically the interdiffusion length and the number of atom displacements in the film [13]. Such process is obviously involved in the focused Ga^+ ion beam (FIB) technique used to magnetically pattern ultrathin film at the nanoscale [3]. Heavy ions (Ga^+, Ar^+, Ne^+) irradiation have been used recently for modifications of exchange coupling between Co layers [14, 15].

Since few years, the influence of the uniform Ga^+ ions bombardment on properties of Pt/Co/Pt layers has been studied also for $d_{\mathrm{Co}} > d_{SRT}$ for nanostructures deposited by either sputtering [16–18] or molecular beam epitaxy (MBE) [19– 22] techniques. Using a wide range of ions

*corresponding author; e-mail: jo@uwb.edu.pl

fluence F (up to ion-driven nanostructure erosion) we have found some new phenomena, such as: (i) existence of two regions with increased magnetic anisotropy, usually connected with increased out-of-plane remnant magnetization, named "branch 1 and 2" in the (d_{Co}, F) phase diagram [22]; (ii) enhanced magneto-optical effects [21, 22]. Two branches of increased magnetic anisotropy and enhanced Kerr rotation were observed after performing both Ga^+ and He^+ ions bombardment of Pt/Co/Pt [13]. However, only the Ga^+ irradiation induced the creation of two PMA branches of out-of-plane magnetization state [19]. X-ray absorption spectra (XAS), X-ray magnetic circular dichroism (XMCD), and extended X-ray absorption fine structure (EXAFS) techniques [17, 20, 22, 23], as well as classical molecular dynamics and Monte Carlo simulations [24], were used for studies of Ga-ions-driven modification of Pt/Co/Pt structures. These changes in magnetic properties were interpreted by considering the competition between the interface and the bulk contributions, the last one being attributed to disordered or ordered CoPt alloys formation [22], lattice stresses [17, 24] and Co-platelet formation [20]. Most of works were done on samples deposited by MBE technique. The influence of Ga ions beam bombardment on magnetic properties of sputtered Pt/Co/Pt was studied only in limited F range [16], i.e. only the branch 1 existence was reported. One can expect that the new phenomena observed for the uniform Ga^+ irradiation could open novel routes for patterning of magnetic nanostructures, especially while applying the FIB technique.

The first goal of the present article is to compare the uniform 30 keV Ga^+ ion-irradiation-induced magnetic changes in Pt/Co(d_{Co})/Pt sputter-grown films with those ones previously reported for their MBE-grown counterparts [22], for both out-of-plane ($d_{\mathrm{Co}} < d_{SRT}$) and in-plane ($d_{\mathrm{Co}} > d_{SRT}$) magnetized pristine films [6]. Sputtering is an important technique of deposition of magnetic nanostructures. Generally, one can expect that the sputtering and MBE preparation methods lead to quantitative different magnetic properties of Co/Pt films [25, 26]. The interface-lateral-correlation length for MBE-grown multilayers is one order of magnitude larger than for sputtered samples [27, 28].

The second goal of the present study is to probe and compare the dependence of magnetic properties of out-of-plane Pt/Co(1.4 nm)/Pt or in-plane Pt/Co(3 nm)/Pt magnetized sputtered films on irradiation by 30 keV Ga^+ ions for the two different, purely uniform or quasi-uniform FIB modes. In the quasi-uniform mode, the FIB is rapidly scanned over all the investigated film area. Some preliminary results were reported for sputtered Co ($d_{\mathrm{Co}} = 1.4$ nm) [13, 29] and Co ($d_{\mathrm{Co}} = 2.6$ nm) [16] films. We evidenced rather similar magnetic changes by both irradiation procedures at comparable estimated fluences while the incoming Ga^+ ion rate in a nanosize region is much higher for the FIB procedure than for uniform irradiation. This result is far to be intuitive since the diffusion length of ions can strongly differ for both procedures. It has to be noticed that no quantitative comparison between uniform and FIB irradiation has been reported so far in spite of its relevance to nanodevice fabrication [3, 30, 31].

The article is organized as follows. The preparation and ion-induced structural modifications in sputtered films are described in Sect. 2. Section 3 is devoted to the study of magnetic properties of uniformly and quasi-uniformly FIB irradiated Pt/Co(3 nm)/Pt and Pt/Co(1.4 nm)/Pt sputtered films by polar Kerr rotation (PKR) magnetometry, and to visualize out-of-plane magnetized domains by polar Kerr microscopy or magnetic force microscopy (MFM). Since the majority of magnetic measurements reported in the present paper were done in configuration when magnetic field is perpendicular to sample surface (out-of-plane configuration), it will not be mentioned explicitly in the experiments description. The term remnant (or residual) magnetization state means in our paper the state obtained after switching off external magnetic field saturating sample in the direction perpendicular to the plane. The mechanisms of irradiation-induced changes in the films and the comparison between quasi-uniform FIB and uniform processes are briefly discussed in Sect. 4. A short conclusion follows in Sect. 5.

2. Ga^+ ion irradiation procedures and expected modifications in Pt/Co/Pt sputtered films

As introduced above, and for the purpose of the present study, two kinds of irradiation procedures were used to modify magnetic properties of sputter deposited Pt(3.5 nm)/Co(3.0 or 1.4 nm)/Pt buffer(4.5 nm) films deposited in high vacuum on a (0001) sapphire substrate [32]:

(i) uniformly irradiated 1 mm wide contiguous (contacting) stripe areas were designed by a step-movable shutter system placed inside a chamber of standard ion implanter for large area irradiation. The fluence, F, was increased by successive steps from 5×10^{12} to 10^{16} Ga^+ ions/cm^2. Alternatively, uniformly Ga^+ irradiated square areas (100×100 μm^2) were prepared through windows indented in a Cu foil mask.

(ii) so-called quasi-uniformly FIB irradiated 50×50 μm^2 or 10×10 μm^2 square areas were designed as a set of parallel overlapping FIB lines while each line consisted of series of irradiation spots (raster scanning) [26]. For a fixed ion beam current, $I = 30$ pA, the spot diameter at the sample surface was $D = 5$ nm [28]. Thus, for quasi-uniform irradiation the separations between two spots along a line and between neighboring lines were selected to be equal to the spot diameter, i.e. 5 nm, in order to obtain a compromise between spot-to-spot fluence variation and total process time.

In the used quasi-uniform FIB irradiation procedure with an ion beam current I during dwell time t_p (time spent FIB per point) is defined linear ion density F_L as $F_L = It_p/D$, which is related with a fluence F as $F = It_p/(eD^2)$, where e is the elementary charge. In the used experimental conditions, the dwell time

$t_p = 1.33$ μs/point, leads to $F = 10^{15}$ Ga^+ ions/cm^2 and $F_L = 0.08$ nC/cm. The number of ions per FIB point, $N = It_p/e$, was then equal to 250 at this fluence. In the used FIB procedure, F_L was varied from 0.02 nC/cm to 1 nC/cm that corresponded to a mean number of 62 to 3100 Ga^+ ions per spot. To adjust the fluence, the dwell time was then varied between 0.33 and 16.6 μs. In our case, $F_L = 0.1$ nC/cm was corresponding to a mean fluence $F = 1.25 \times 10^{15}$ Ga^+ ions/cm^2. In the following, we will tentatively use this relation to compare the effects of uniform or quasi-uniform FIB irradiation modes.

More difficult is to evaluate the uniformity of the fluence inside a FIB spot. First, ion current radial distribution is not uniform but rather Gaussian. Second, SRIM simulations [33] indicated that the density of collision events in the FIB spot section exhibited radial straggle with a nearly Gaussian lateral profile [3] but with a width at half amplitude 8 nm is larger than its diameter. Thus, if the magnetic exchange length is significantly smaller than radial straggle (for non-irradiated cobalt magnetic exchange length is order of 3 nm), non-uniform magnetic properties may be induced inside the FIB irradiated spot area.

Considering an approximation of uniform collisions events and an ion beam current $I = 30$ pA, we deduce a delay of about 5 ns between two successive ion impacts, which is significantly longer than the cascade thermal relaxation time determined from molecular dynamic simulations [24]. But after the thermalization, subsequent processes at the ambient temperature, such as thermally activated motion of defects generated previous ion impact, may occur in delayed stage for a period exceeding 1 ns [34]. Thus in our experimental conditions, full stabilization of intermixing processes between successive ion impacts cannot be achieved. Besides it, FIB irradiation is characterized by much deeper ion penetration that it was expected from classical collision model for uniform irradiation [35].

Let us try now to predict mixing created inside the film structure. TRIDYN simulations [36] are the most usual way to get a rough view of the variation of the in-depth Co and Pt composition and the amount of implanted Ga^+ ions in the film structure. Unfortunately, especially for irradiation by heavy ions, they do not consider the formation of voids and the possible thermodynamic formation of stable alloy structures. Thus, real damages at relatively high fluence are surely more drastic than those predicted by TRIDYN simulations. Nevertheless, at least at small fluence, they give some insight on in-depth alloying and consequently on expected changes in magnetic properties [13]. Results for typical Ga^+ ion fluences of 10^{14} ions/cm^2 and 4×10^{14} ions/cm^2 on the Al_2O_3/Pt(4.5 nm)/Co(3 nm)/Pt(3.5 nm) in-depth film structure are presented in Fig. 1: (a) At very low fluence ($F = 10^{14}$ Ga^+ ions/cm^2: Fig. 1a), intermixing of Co and Pt ions already appears at Co/Pt interfaces, (b) at a slightly higher fluence ($F = 4 \times 10^{14}$ Ga^+ ions/cm^2: Fig. 1b), i.e. in the "branch 1" region [22],

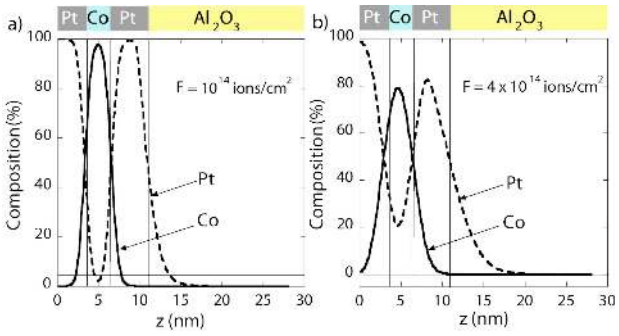

Fig. 1. Results of TRIDYN simulations: in-depth composition profile of Co and Pt ions in the Pt(3.5 nm)/Co(3 nm)/Pt(4.5 nm)/Al_2O_3 film for two characteristic fluences, F. Part (b) relates to "branch 1" of the phase diagram [13]. The curves in (a) and (b) are non-symmetric because Ga^+ ions are progressively less energetic when propagating inside the film structure. On the top of each figure a scheme of the pristine stack is indicated. The initial positions of the interfaces are marked by vertical lines. $z = 0$ corresponds to the as-deposited film surface position.

intermixing effects spread more and the composition of Co or Pt are different at the two buried interfaces.

At much higher fluence (8×10^{15} ions/cm^2) a complete intermixing of Co and Pt ions is predicted inside the full structure. It should be noted that while less than 1% Ga^+ ions are implanted in the Co–Pt region for $F < 7 \times 10^{15}$ Ga^+ ions/cm^2, TRIDYN calculations predict that ion etching effects occur only at the surface of the Pt overlayer (together with intermixed there Co), while at much higher fluence etching can reach the Co layer. Mean penetration depth for Ga^+ ions from TRIDYN simulation is about 10 nm.

The optical reflectivity in uniformly irradiated (100×100 μm^2) square areas is progressively reduced when increasing the fluence, in agreement with the enhancement of the film transmission associated with sample etching [29]. As previously checked [37] and presently confirmed by AFM on a uniformly irradiated sputtered film, the surface roughness was slightly enhanced by a factor of about two between $F = 0$ and $F = 7 \times 10^{14}$ Ga^+ ions/cm^2. This was confirmed on quasi-homogeneously FIB irradiated areas. As the result of a huge sample etching, in the range between $F = 7$ and 12.5×10^{15} Ga^+ ions/cm^2 the mean roughness was markedly increased by a factor 5. X-ray reflectivity for both MBE and sputtered films also reveals an increase in thickness of the interfaces up to 0.5–1 nm.

3. Magnetic properties and magnetization states of Ga^+ irradiated Pt/Co(3 nm)/Pt and Pt/Co(1.4 nm)/Pt sputtered films

3.1. Magnetic properties of as-grown Pt/Co(d_{Co})/Pt films

The d_{Co}-dependence of the coercive field and the effective anisotropy field of as-grown sputtered films is

quite similar to these found for MBE grown films (see Fig. 3a in Ref. [22]). The value of the SRT critical thickness at room temperature for MBE grown films (d_{SRT} = 2.2 nm) [22] is nevertheless larger than for sputtered films (d_{SRT} = 1.7 nm) [6]. As previously reported [13], the as-grown Pt/Co(1.4 nm)/Pt sputtered film ($d_{\mathrm{Co}} < d_{SRT}$), exhibits a square magnetic hysteresis loop at room temperature consistent with a rather large anisotropy field H_A^{eff} = 1.9 kOe. On the contrary, for thicker Co layers ($d_{\mathrm{Co}} > d_{SRT}$) with in-plane anisotropy, d_{Co} = 2.6 nm [16] or d_{Co} = 3.0 nm (Fig. 2a), a pure S-shape field induced magnetization curve without hysteresis and with high saturation field was measured.

3.2. Magnetic and magneto-optical properties of uniformly Ga^+ irradiated Pt/Co(3.0 nm)/Pt sputtered films

When increasing the Ga^+ ion fluence F, similarly as for the MBE grown film [22], the sputtered Pt/Co(3 nm)/Pt sample depicts two successive regions (labeled "branches 1 and 2") with out-of-plane magnetized component. This is supported by hysteresis loop measurements (Fig. 2b,e). Only the first in-plane to out-of-plane SRT had been previously evidenced at low fluence in a sputtered d_{Co} = 2.6 nm film [16]. Similarly, in the new d_{Co} = 3 nm sputtered film, SRT is first induced at low fluence over a reduced $1 < F < 5 \times 10^{14}$ Ga^+ ions/cm^2 range (Fig. 2b) (1$^{\mathrm{st}}$ SRT — "branch 1"), the remnant magnetization becoming equal to the saturated magnetization for $F \approx 4 \times 10^{14}$ Ga^+ ions/cm^2 (Fig. 3). In the $F = 0.8 - 6 \times 10^{15}$ Ga^+ ions/cm^2 range, the remanence falls to zero but magnetization still indicates an out-of-plane component while it is essentially oriented in-plane (inset of Fig. 2c). The pronounced curvature of the loop (Fig. 2c) could be explained by the presence of multidomain structure with out-of-plane magnetization [38] or mentioned above coexistence of two magnetization phases. Finally, for $6 \times 10^{15} < F < 9 \times 10^{15}$ Ga^+ ions/cm^2 ("branch 2"), a nonzero remanence emerges as the consequence of the reappearance of a net normal component of the magnetization. The most abrupt variation of the PKR signal at small field is then observed for $F = 8.75 \times 10^{15}$ Ga^+ ions/cm^2 (Fig. 2e); it is accompanied by a weak hysteresis (Fig. 2e) with a non-saturated remnant state (Fig. 3). Further increase of the fluence F results in: (i) decrease of both hysteresis and amplitude of magnetization loop, see Fig. 2f for $F \approx 10^{16}$ Ga^+ ions/cm^2; (ii) sample etching which could be determined from simulations and experiments [29]. Before final nanostructure etching, the samples undergo transition into superparamagnetic state — separated magnetic grains in nonmagnetic matrix.

For pristine films with in-plane oriented magnetization ($d_{Co} < d_{SRT}$), the effective anisotropy field H_A^{eff} was determined from the saturation field of the PKR based on a simple easy axis model accounting phenomenologically of only one magnetic anisotropy constant. Magnetic anisotropy in regions with perpendicular anisotropy

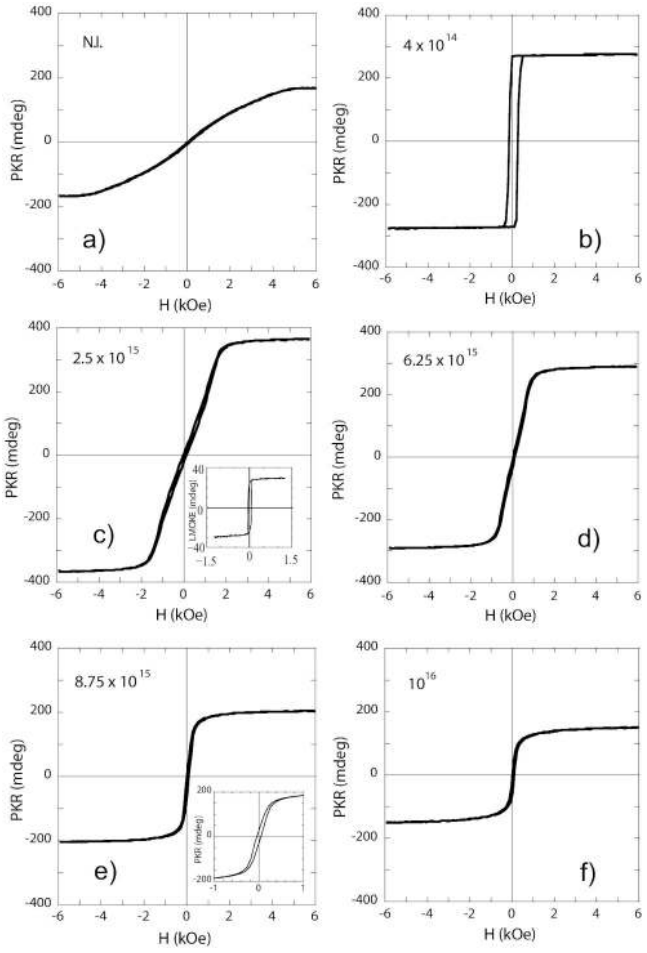

Fig. 2. PKR loops of (a) the as-grown non-irradiated (N.I.) Pt/Co(3 nm)/Pt sputtered film, or (b)–(f): uniformly irradiated with increasing fluence, F, indicated in Ga^+ ions/cm^2 units. The inset of (c) shows the longitudinal MOKE (LMOKE) hysteresis loop indicating the presence of an in-plane magnetization component. The inset of (e) (zoom of the $H = 0$ area) reveals a weak hysteresis.

was determined analyzing rotational part of magnetization curves in crossed out-of-plane and in-plane magnetic fields following procedure similar as was discussed in the work [39]. For the d_{Co} = 3 nm sputtered film, the dependence of H_A^{eff} with the Ga^+ ion fluence is depicted in Fig. 4. It displays similar trends than that found previously for a thinner d_{Co} = 2.6 nm sputtered film [16], or for thick ($d_{\mathrm{Co}} > d_{SRT}$) MBE grown films (see Fig. 3a of Ref. [22]). One can find unexpected results — the coexistence of out-of-plane remnant magnetization (Fig. 3) and negative value of anisotropy field H_A^{eff} (Fig. 4). The creation of magnetization phases (in nanometer scale, so it is below our experimental setups spatial resolution) with different magnetic anisotropy can explain these results.

As reported for the uniformly irradiated Pt/Co(2.6 nm)/Pt sputtered film [16] with $F \approx 10^{14}$ Ga^+ ions/cm^2, a maze-like remnant out-of-plane domain pattern for an ac-demagnetized state (after demagneti-

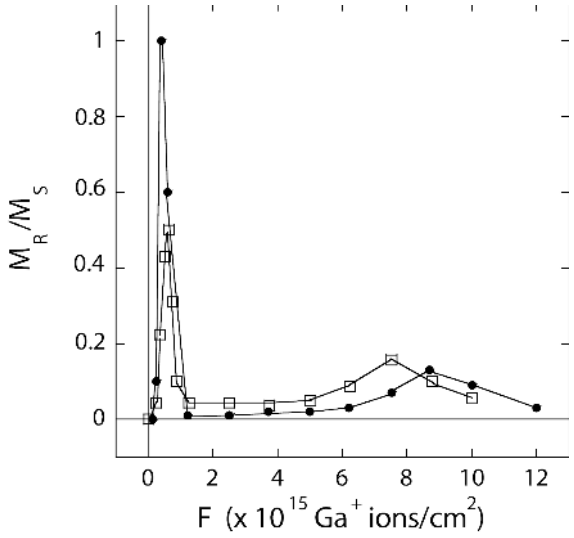

Fig. 3. Variation of the normalized remnant magnetization with the Ga^+ ion fluence for the uniformly (•) or FIB irradiated (□) Pt/Co(3 nm)/Pt sputtered film. The lines are guides for the eyes.

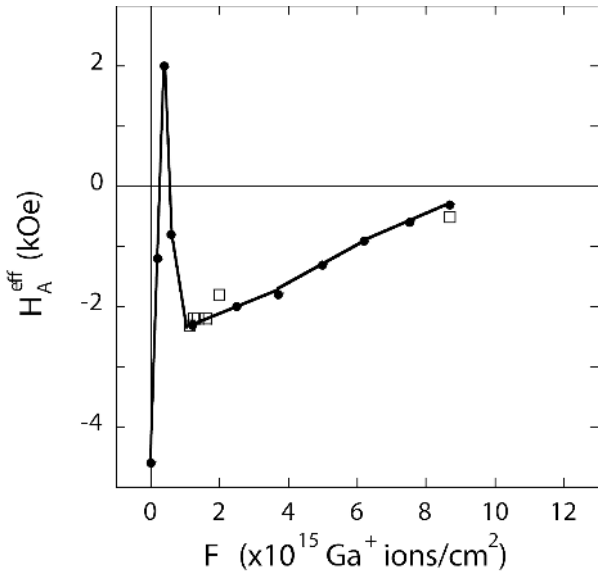

Fig. 4. Variation of the measured effective anisotropy field with the Ga^+ ion fluence for the uniformly irradiated (•) or FIB irradiated sputtered film (□) Pt/Co(3 nm)/Pt sputtered film. The line is a guide for the eyes. Data were obtained with fitting the reversible parts of the hysteresis loops with an easy axis model including only one magnetic anisotropy constant.

zation in out-of-plane decaying ac magnetic field) like observed by MFM on the irradiated Pt/Co(3 nm)/Pt sputtered film irradiated with $F = 4{\times}10^{14}$ Ga^+ ions/cm^2 (Fig. 5a). The MFM image in Fig. 5b reveals a complex up-down (black and white) out-of-plane demagnetized domain structure that appears at the boundary (transitional zone) between two in-plane magnetized states, one being non-irradiated (right) and the other just irradiated

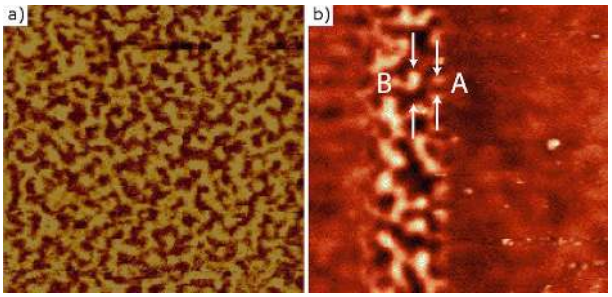

Fig. 5. MFM images of the domain structure in the Pt/Co(3 nm)/Pt sputtered film: (a) uniformly irradiated with $F = 4 \times 10^{14}$ Ga^+ ions/cm^2, (b) out-of-plane magnetized domain state at the boundary between $F = 2.5 \times 10^{15}$ Ga^+ ions/cm^2 (left) irradiated and $F = 0$ (right) non-irradiated regions with in-plane anisotropy. The image sizes are respectively 5×5 μm^2 for (a) and 10×10 μm^2 for (b). Arrows pairs indicate on the domain size at the border between out-of-plane and in-plane magnetization state (A) and at the center (B) of the stripe.

with $F = 2.5 \times 10^{15}$ Ga^+ ions/cm^2 (left). Domains size (B) decreases down to few hundreds nanometers (A) while approaching the border between out-of-plane and in-plane magnetization state (SRT region). Submicrometer domain sizes near SRT were theoretically predicted in [40–42]. This domains behavior is consistent with the fluence gradient present across the transitional zone between the two regions that involves intermediate fluences belonging to branch 1. Changing the fluence F and the mask–sample distance, one can control the lateral expansion of this PMA boundary ribbon.

The magnetization reversal process at the boundary between two regions with in-plane anisotropy, i.e. an irradiated one with $F = 10^{15}$ Ga^+ ions/cm^2 (F just above the branch 1) surrounded by a non-irradiated (N.I.) film area has been also investigated by polar magneto-optical Kerr effect (PMOKE) microscopy on the irradiated Pt/Co(3 nm)/Pt sputtered film (Fig. 6). The field was applied perpendicular to the film plane. The width of the PMA boundary is in the micrometer range, so it is rather difficult to determine local magnetization by conventional PMOKE hysteresis measurements. Thus, for magnetization reversal studies we used the 3 steps procedure of remnant hysteresis loop measurement [43], schematically shown in Fig. 6c: (i) a reference image of the remnant magnetization state was first recorded at t_0 after saturating the sample in a large negative field of – 4 kOe bigger than coercivity field H_C; (ii) a set of images of the remnant magnetization states was acquired after applying a sequence of square field pulses with amplitude H following to the linear sweep in classical hysteresis loop measurements (red dashed line); (iii) the final remnant field-induced images (Fig. 6a,b) were obtained by subtracting set of images (ii) and reference (i). After applying $H = 300$ Oe, the magnetization reversed only at some places in the boundary which appeared as "black" ribbons segments (Fig. 6a). As revealed on the

(iii) image for $H = 500$ Oe (Fig. 6b), the magnetization saturated rapidly in the boundary and stabilized in the remnant state. The remnant magnetization loop of a short boundary segment was constructed from the integrated PMOKE intensity over few pixels of the camera (Fig. 6d). This hysteresis loop was non-symmetric because reversal was non-reproducible for a short part of the boundary. Note that the central irradiated area with $F = 10^{15}$ Ga^+ ions/cm^2 shows a granular inhomogeneous remnant magnetic state (Fig. 6a,b) with a weak perpendicular magnetization component.

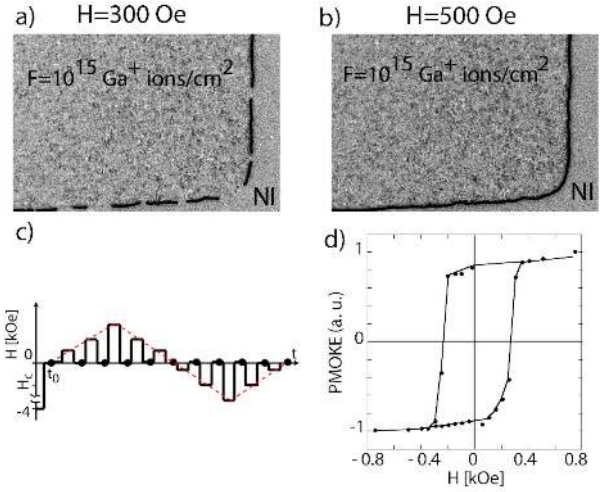

Fig. 6. PMOKE images (85×55 μm^2) of the magnetization reversal in the boundary between in-plane irradiated (upper left) and non-irradiated (N.I., down right) magnetized regions. (a, b) Remnant images after processing and obtained after the application of fields indicated above the images. (c) Time sequence of the pulse magnetic field to obtain remnant hysteresis loop for stripe boundary. Black points indicate the times of PKR image acquisition. Red dashed line corresponds to the magnetic field evolution during classical hysteresis loop measurement. (d) Remnant hysteresis loop deduced from PKR integrated intensity inside a short segment of the boundary (line is only a guide for the eyes).

As already quoted for some sputtered [16] or MBE grown [22] films, the magnitude of polar magneto-optical effects at saturation for uniformly Ga^+ irradiated in-plane magnetized pristine films with $d_{Co} > d_{SRT}$ increases first with the fluence to rapidly reach a maximum and decreases above (Fig. 7). For example, this irradiation-induced behavior for the PKR depends on changes in optical properties and is indirectly linked to the competition between volume and interface spin–orbit contributions. Since different polar magneto-optical effects (ellipticity or rotation) carried out either in light transmission or reflection relate to different combinations of the optical and magneto-optical parameters, the same tendency was found but with different efficiency, meaning that the fluence corresponding to the maximum magneto-optical effect was dependent upon the measured magneto-optical observable.

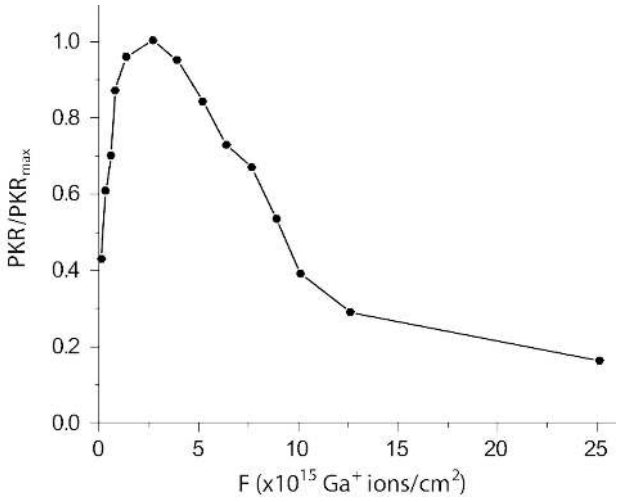

Fig. 7. Variation of the saturated PKR signal at 640 nm in a uniformly Ga^+ ion irradiated sputtered Pt/Co(3 nm)/Pt film.

3.3. Magnetic and magneto-optical properties of quasi-uniformly FIB irradiated Pt/Co(3.0 nm)/Pt sputtered films with initial in-plane magnetization

The magnetic hysteresis loops of quasi-uniformly FIB irradiated (50×50 μm^2) square areas in the Pt/Co(3.0 nm)/Pt sputtered film were measured by PKR for several characteristic fluences (Fig. 8). Remnant hysteresis loops of quasi-uniformly FIB irradiated (10×10 μm^2) square areas were also deduced, for branches 1 and 2, from the measured PKR image intensity recorded after switching off the field (Fig. 9). Similar trends were found either for the uniformly (Sect. 3.2) or quasi-uniformly FIB irradiated Co(3 nm) sputtered films. Let us precise the behavior of the FIB irradiated ones:

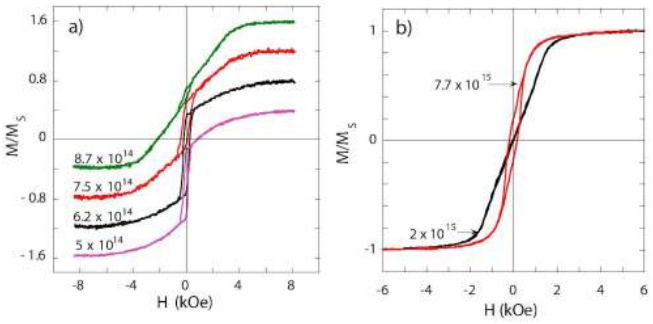

Fig. 8. Normalized PKR hysteresis loops of the quasi-uniformly FIB irradiated Pt/Co(3 nm)/Pt sputtered film for (a) low, (b) medium and high fluences. The fluence is indicated in Ga^+ ions/cm^2 units. For clarity, the curves in part (a) are shifted along the vertical direction.

(i) at low fluence (in the 10^{14} Ga^+ ions/cm^2 range), a square hysteresis loop with small coercivity (≈ 200 Oe) and large amplitude (about $0.5M_S$ — it was M_S for

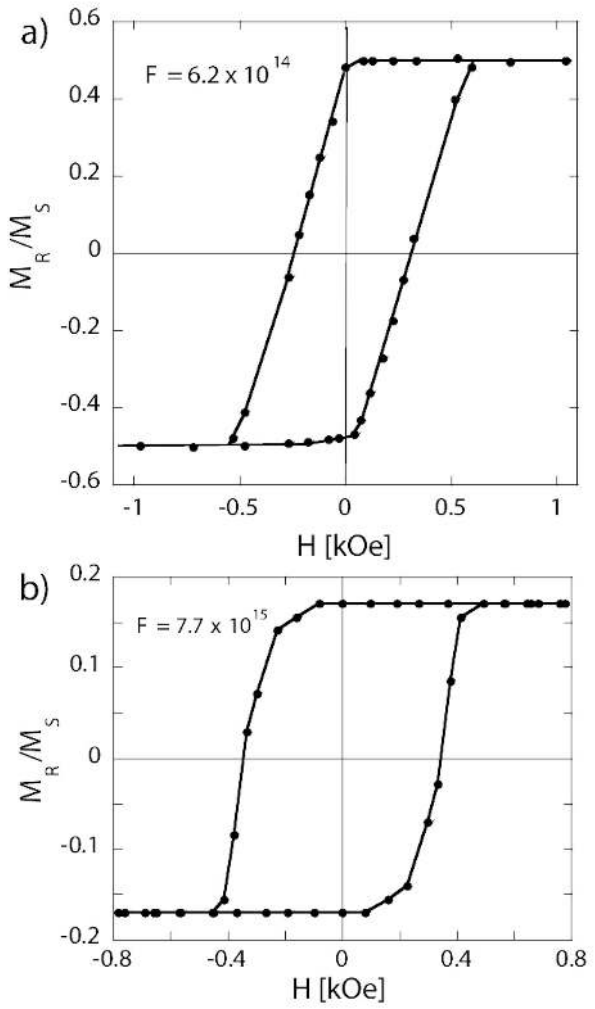

Fig. 9. Remnant hysteresis loops deduced from PKR image processing in (a) (50×50 μm^2), or (b) (10×10 μm^2) quasi-uniformly FIB irradiated areas in the Pt/Co(3 nm)/Pt sputtered film for two typical mean fluences (F in Ga^+ ions/cm^2) that induce perpendicular anisotropy (branches 1 and 2).

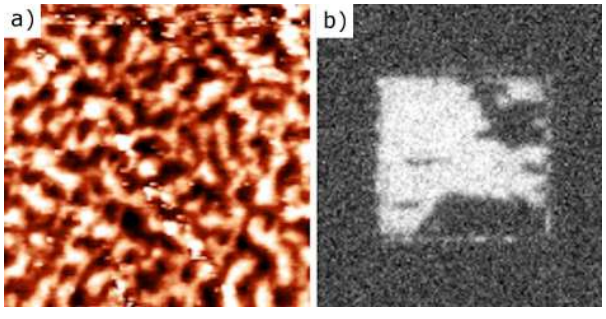

Fig. 10. ac-demagnetized states in quasi-uniformly FIB irradiated areas in the Pt/Co(3 nm)/Pt sputtered film. (a) MFM image (10×10 μm^2) for $F = 5 \times 10^{14}$ Ga^+ ions/cm^2; (b) PKR image of a central square area (10×10 μm^2) irradiated with $F = 7.7 \times 10^{15}$ Ga^+ ions/cm^2. Large remnant domains with up and down magnetization can be visualized.

the uniformly irradiated film) is superimposed on an in-plane contribution (Fig. 8a). Accordingly, a large signal was measured from the remnant PKR image intensity (Fig. 9a),

(ii) at intermediate fluence (in the 0.8 to 5×10^{15} Ga^+ ions/cm^2 range), the magnetization lies nearly in-plane (Fig. 8b),

(iii) at high fluence (in the 5 to 9×10^{15} Ga^+ ions/cm^2 range), a low field hysteresis loop was evidenced (Fig. 8b), according to a partial SRT toward the film normal. The remnant PKR hysteresis loop confirms the onset of a stable perpendicular magnetization component (Fig. 9b).

Thus, two successive SRTs to PMA states are still evidenced when increasing the fluence up to finally reach superparamagnetism. The existence of remnant magnetic domain structures (Fig. 10a,b) confirms the stability of these PMA states with rather large perpendicular magnetization components. Considering the uncertainty (20%) on the estimated correspondence between fluences and linear ion density (Sect. 2), we can consider that the M_R/M_S ratio (Fig. 3) and the effective anisotropy H_A^{eff} (Fig. 4) exhibit a comparable behavior with the mean Ga^+ ion fluence for either the uniformly irradiated or quasi-uniformly FIB irradiated Co(3.0 nm) films. These trends also hold for the previously studied Pt/Co(2.6 nm)/Pt sputtered film [16], or MBE grown films [22]. As in uniformly irradiated squares (Fig. 5b), remnant perpendicular magnetization can be still stabilized at the boundary between two different in-plane magnetized non-irradiated and highly irradiated film regions, confirming the existence of a perpendicular remnant state at intermediate fluence.

3.4. Magnetic and magneto-optical properties of uniformly and FIB irradiated Pt/Co(1.4 nm)/Pt sputtered films with initial out-of-plane magnetization

The changes of magnetic properties of quasi-uniformly FIB irradiated (80×80 μm^2) areas in a ($d_{Co} < d_{SRT}$) Pt/Co(1.4 nm)/Pt sputtered film with out-of-plane magnetization deposited on a sapphire substrate have been partly discussed [13]. For comparison, new data were obtained on the same film but now uniformly irradiated by Ga^+ ions at several characteristic fluences. The irradiation procedure was similar to that used for the Co(3 nm) film (Sect. 2), i.e. contiguous 1 mm wide stripes were irradiated step by step with fluence varying between 5×10^{12} to 1.2×10^{15} Ga^+ ions/cm^2.

Irradiation-induced magnetic changes were found to be nearly similar to those reported in uniformly irradiated Pt/Co(1.4 nm)/Pt sputtered films and can be listed as follows. The pristine film exhibits PMA that provides a highly square hysteresis loop (Fig. 11a). Its coercive field is reduced under irradiation (Figs. 11b,c and 12) up to reach a superparamagnetic state above $F \approx 10^{15}$ Ga^+ ions/cm^2 (uniform irradiation) or $F \approx 0.9 \times 10^{15}$ Ga^+ ions/cm^2 (quasi-uniform FIB irradiation). These are usual behaviors exhibited after irradiation of ultrathin ($d_{Co} < d_{SRT}$) Co/Pt films with PMA [3]. Our new

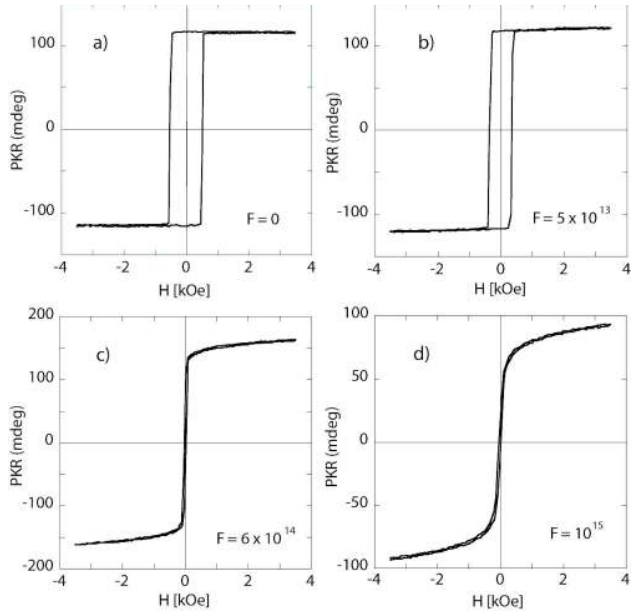

Fig. 11. PKR hysteresis loops of the Pt/Co(1.4 nm)/Pt sputtered film: (a) non-irradiated, or (b)–(d) uniformly irradiated with Ga^+ ions for increasing fluences, F, indicated in Ga^+ ions/cm^2 units.

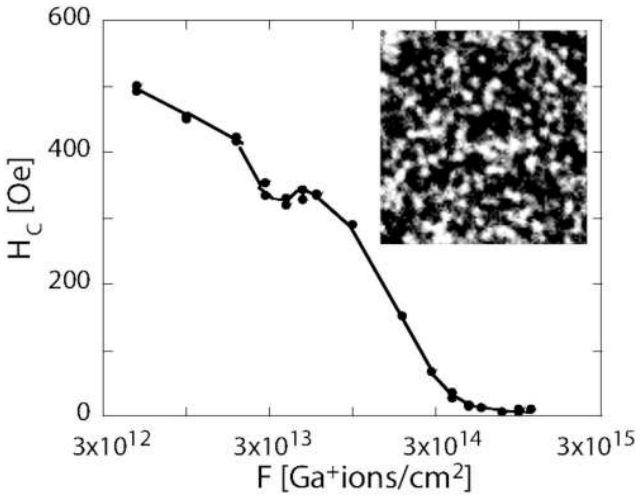

Fig. 12. Uniformly Ga^+ ion irradiated Pt/Co(1.4 nm)/Pt sputtered film: variation of the coercive field with the fluence. Inset: PKR image of the ac-demagnetized domain state ($F = 2.5 \times 10^{14}$ Ga^+ ions/cm^2, image size 50×50 μm^2).

results under uniform irradiation have evidenced a local decrease of the coercivity in the $10^{13} < F < 10^{14}$ fluence range, consistently with the re-entrant behavior shown for MBE grown films in the expected branch 1 region (see Fig. 3a of Ref. [22]). As already found in MBE-grown films with PMA [22], an up-down out-of-plane ac-demagnetized domain structure was observed in FIB irradiated squares at low fluence (Fig. 12, inset).

As previously found in the quasi-uniformly FIB irradiated film [13], the amplitude of the magnetic hysteresis square loop decreases upon irradiation at the expense of a reversible S-shaped magnetization curve contribution evidencing a progressive out-of-plane to in-plane reorientation of the magnetization and/or demagnetizing domain structure like in [44] (Fig. 13). In the uniformly irradiated sputtered film, the PMA was described by the effective anisotropy field H_A^{eff}, determined by analyzing

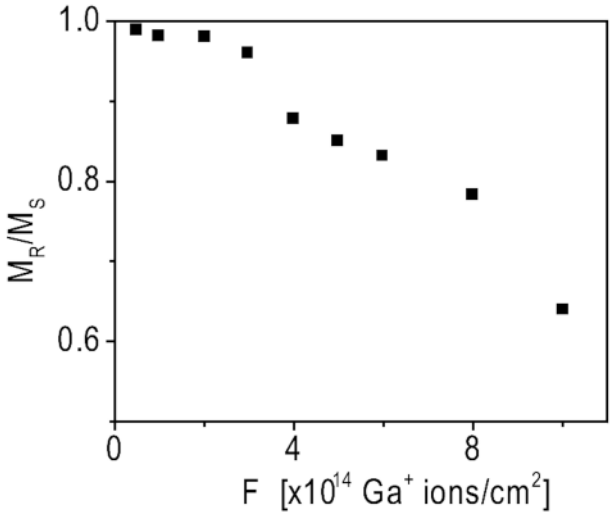

Fig. 13. Uniformly Ga^+ ion irradiated Pt/Co(1.4 nm)/Pt film: the variation of the normalized remnant magnetization M_R/M_S with the fluence.

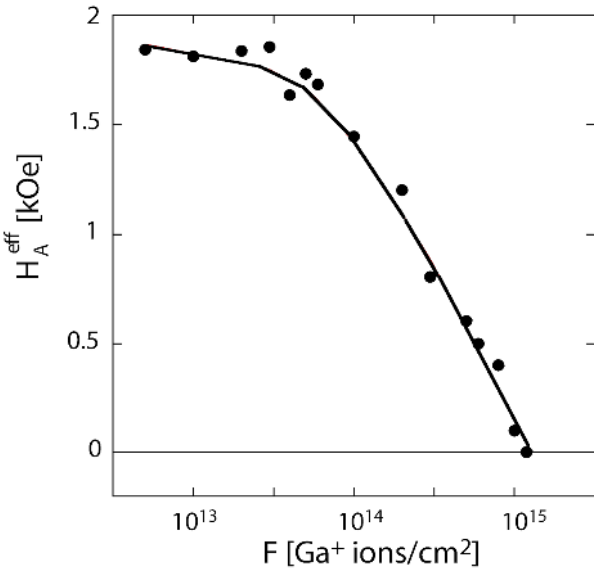

Fig. 14. Variation of the effective anisotropy field, H_A^{eff}, of the uniformly Ga^+ irradiated Pt/Co(1.4 nm)/Pt sputtered film with the fluence in a semilogarithmic plot.

rotational part of magnetization curves in crossed out-of-plane and in-plane magnetic fields [39]. The PMA is found to be nearly constant with the fluence up to $F \approx 4 \times 10^{13}$ Ga^+ ions/cm^2 and decreases monotonously above (Fig. 14) to vanish around 10^{15} Ga^+ ions/cm^2. This last result is consistent with the anisotropy variation found for the FIB irradiated film [13]. In agreement with previous results in a FIB irradiated film [13], the amplitude of the saturated PKR in the uniformly irradiated film increases first with the fluence up to reach a maximum for $F \approx 2 \times 10^{14}$ Ga^+ ions/cm^2 ($F \approx 3 \times 10^{14}$ Ga^+ ions/cm^2 for the FIB irradiated film) and decreases at higher fluence (Fig. 15). This behavior was also found for sputtered $d_{Co} > d_{SRT}$ films (Fig. 7), and even in the MBE grown Pt/Co(1.4 nm)/Pt film [22].

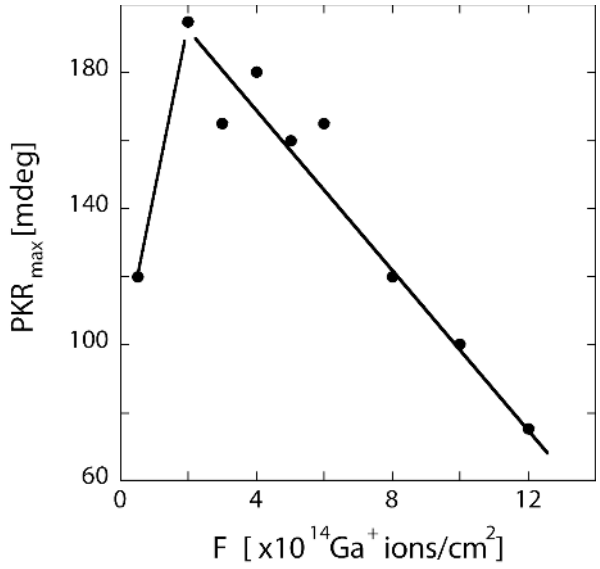

Fig. 15. Variation of the saturated PKR amplitude at 640 nm for the uniformly irradiated Pt/Co(1.4 nm)/Pt sputtered film with the fluence. The straight lines are guides for the eyes.

4. Origins of the irradiation-induced changes of magnetic characteristics of the films

One has first to examine the role of implanted Ga^+ ions from the source, and of Al and O atoms diffused in the film from the sapphire substrate. For example, after uniform ion irradiation at rather high fluence of $F = 8 \times 10^{15}$ Ga^+ ions/cm^2, TRIDYN simulations show that only a few % of Ga^+ ions are implanted close to the Pt buffer layer/sapphire interface. Thus, one can imagine that magnetism could be seriously affected by structural and textural changes. This was definitively not the case since we demonstrated that the induction of two successive PMA phases (in branch 1 and 2) when increasing the fluence in a pristine film with in-plane magnetization is not very sensitive to the amount of Ga^+ ions and O, and Al atoms implanted in the film structure, as checked in two other different MBE grown film structures with either thick Pt(20 nm)/Mo(20 nm) [22] or Pt(20 nm) [19] buffer layers directly deposited on sapphire. In these last cases Ga^+ implants far away from the sapphire substrate. Thus, since the magnetic changes in the sputtered or the two MBE-grown films are similar, they are essentially related to modifications at Co/Pt interfaces or inside the Co layer, but not directly to Ga^+ implantation or diffusion of atoms from the sapphire substrate.

The processes giving rise to PMA at low (branch 1) and high (branch 2) Ga^+ ion fluence have different origin. In the branch 1 region [23], cross-sectional TEM investigations confirm the existence of parts with regular crystal structure while such structure is not present in the branch 2 region. For branch 1, X-ray reflectivity measurements reveals Co–Pt intermixing at the interfaces, but the etching phenomenon in the Pt overlayer together with intermixed Co is dominating for branch 2. These basic phenomena were often predicted in other systems. It is still a challenge to experimentally determine the microscopic processes accompanying the apparition of PMA under Ga^+ ion irradiation because this needs to check locally the structure and magnetism at the nanoscale. The magnetic changes under Ga^+ ion irradiation in Pt/Co(d_{Co})/Pt sputtered films with as-grown in-plane anisotropy ($d_{Co} > d_{SRT}$) can be interpreted as three consecutive effects arising from the competition between interface and volume phenomena.

First, under low fluence ($F = 1$ to 4×10^{14} Ga^+ ions/cm^2), at least two possibilities are offered for interpreting the apparition of PMA and stable remnant perpendicular magnetization (i.e. in branch 1) under irradiation both in the sputtered or MBE grown Pt/Co(3 nm)/Pt films: (i) the irradiation-induced in-plane lattice expansion [17, 24], (ii) the irradiation-induced formation of high anisotropy species near disturbed Co/Pt interfaces. For the item (ii), structural changes are driven by collision cascades of ions that generate thermal spikes inside which the temperature rises up to several thousand kelvins, i.e. far above the metallic melting temperature [45–49]. For metallic compounds, it was known that order/disorder transitions can occur under irradiation, but for long range disorder/order transition additional thermal annealing during or after irradiation is necessary [50, 2]. Recent spectroscopic magneto-optical investigations [18] revealed a negative PKR peak at 3.2 eV in a comparable weakly irradiated (in branch 1) Pt/Co(2.6 nm)/Pt sputtered film (with $F = 10^{14}$ Ga^+ ions/cm^2) that can be the signature of an hcp $Co_{0.75}Pt_{0.25}$ ordered alloy phase with high magnetic anisotropy, as already reported by several authors [51–54]. According to the simulation results [24] the amount of local chemical ordering phase is not significant but together with induced tensile in-plane strain [17, 24] can explain the restored PMA in the "branch 1" region of the (d_{Co}, F) phase diagram [22].

Second, at moderate fluence ($F = 4 \times 10^{14}$ to 5×10^{15} Ga^+ ions/cm^2), there appears only isotropic Co lattice deformation [17]. Moreover, the PMA interface term is reduced under irradiation favoring intermixing at Pt/Co

interfaces (Fig. 1) [13]. Thus, the magnetization tends to reorient again in-plane at moderate irradiation fluence.

Third, for a higher fluence ($F = 5$ to 9×10^{15} Ga^+ ions/cm^2), the high atomic intermixing and pulverization at the film surface produce an important etching of the sample and formation of Co nanodisks [20] with a single atom thickness. At this stage, two different mechanisms are responsible for the appearance of out-of-plane component: (i) Co–Pt amorphous alloys with high Pt content and having low magnetization and reducing shape anisotropy [55], (ii) anisotropy of Co nanodiscs would enhance out-of-plane magnetic component [56]. Finally, a higher fluence, superparamagnetism appeared and magnetic anisotropy is suppressed. These arguments hold for both the sputtered and MBE grown films.

In the thinner Co(1.4 nm) sputtered film, the PMA does not change at low fluence up to 5×10^{13} Ga^+ ions/cm^2, while it progressively reduces when increasing the fluence up to about 10^{15} Ga^+ ions/cm^2 (Fig. 14). Such transition from smooth out-of-plane magnetization to superparamagnetic state is also depicted in the Co(1.4 nm) MBE grown film [22].

As for MBE grown films [22], the magnitude of all types of magneto-optical effects, measured in either out-of-plane (Fig. 15) or in-plane (Fig. 7) magnetized irradiated sputtered films increases first with the fluence to further decrease. Increase of the magnitude at low fluences can be the indicator of appearance of substitutional alloy at Co/Pt interface with tensile stress, which strongly increases magnitude of magneto-optical effects [57]. At high fluences magnitude is decreasing due to Co dissolving below the concentration of ferromagnetic threshold [13] and/or Co elimination due to ion sputtering.

While the irradiation procedures differ drastically in used ion density current (standard ion implanter operates at about 1 μA/cm^2, FIB — 1 A/cm^2) and mentioned above (Sect. 2) distinctions, we have experimentally demonstrated that uniform or quasi-uniform FIB irradiation of Pt/Co/Pt films give rise to nearly the same qualitative changes of their magnetic properties when using comparable Ga^+ ion fluences.

5. Conclusion

The irradiation fluence driven changes of magnetic anisotropy and enhancement of magneto-optical effects were observed in Pt/Co/Pt layers. Qualitative similar irradiation-induced magnetic changes are evidenced in quasi-uniformly FIB or uniformly irradiated films, grown by sputtering. Similarly as for MBE deposited samples both irradiation procedure induced in sputtered Pt/Co/Pt layers: (i) two Ga ions fluence F regions with increased magnetic anisotropy and increased out-of-plane remnant magnetization, (ii) enhanced magneto-optical effects. The out-of-plane remnant magnetization value in branch 1 was smaller for FIB irradiated samples which is connected with different irradiation conditions (much higher ions density for FIB).

The observed in-plane lattice expansion at low Ga^+ ion fluence [17] can partly explain the onset of PMA in "branch 1" [22], but collision cascades and thermal spikes after fast cooling highly favor the formation of ordered alloys with large magnetic anisotropy. For irradiation at low fluence, magneto-optical spectroscopy results allowed to identify the presence of additional Co–Pt alloy, similar to hcp $Co_{0.75}Pt_{0.25}$ ordered alloy phase [51–54] with huge PMA that can be initiated in the vicinity of Co/Pt interfaces. In the future, more direct experiments would be necessary to make structural confirmation this ordered alloy and its precise spatial profile in the film structure at a nanometer scale. Such an experimental task is rather difficult even for high resolution transmission electron microscopy analysis of film cross-section due to the small ratio of in-plane correlation length hcp $Co_{0.75}Pt_{0.25}$ structure — 0.8 nm [51] to the analyzed slice thickness.

Finally, the fact that uniform or quasi-uniform FIB irradiation creates nearly similar damages and magnetic changes for equivalent fluences is reasonable since processes result from the ultra-fast interaction between incoming Ga^+ ions and the target, even for multicollision processes. In view of applications this result allows us to calculate the Ga^+ ion fluence which is needed to modify magnetic properties in FIB nanostructures in a controlled way [3, 28, 58–65].

The irradiation-induced modification of magnetic and magneto-optical properties opens new possibilities to create novel structures (e.g. shift registers [28] or magnonic crystals) with patterning down to submicrometer sizes easy available using FIB irradiation. Tests of FIB produced small sizes modifications can be performed using experimental techniques enabling large ion modified areas (many square millimeters) obtained by the uniform irradiation.

Acknowledgments

This work was supported by the Marie-Curie ToK NANOMAG-LAB project (No. MTKD-CT-2004-003177) and SYMPHONY project with the Foundation for Polish Science Team Program co-financed by the EU European Regional Development Fund, OPIE 2007-2013. It has also benefited of the EU "Research Infrastructures Transnational Access" program "Center for Application of Ion Beam in Material Research" under Grant No. 025646. J.J. has benefited of an EC Marie-Curie Fellowship Grant No. MEST CT 2004-51437. P.M. was supported in the frame FUGA project, financed by the National Science Centre (DEC-2015/16/S/ST3/00450) and partly by Statutory Found of ICSC PAS. This article has also received financial support from the Polish Ministry of Science and Higher Education under subsidy for maintaining the research potential of the Faculty of Physics, University of Bialystok.

References

[1] C. Chappert, H. Bernas, J. Ferré, V. Kottler, J.-P. Jamet, Y. Chen, E. Cambril, T. Devolder, F. Rousseaux, V. Mathet, H. Launois, *Science* **280**, 1919 (1998).

[2] J. Fassbender, D. Ravelosona, Y. Samson, *J. Phys. D Appl. Phys.* **37**, R179 (2004).

[3] J. Ferré, J.-P. Jamet, in: *Handbook of Magnetism and Advanced Magnetic Materials*, Eds. H. Kronmüller, S. Parkin, Wiley, New York 2007, p. 1710.

[4] T. Devolder, H. Bernas, in: *Material Science With Ion Beams*, series *Topics in Applied Physics*, Ed. H. Bernas, Vol. 116, Springer-Verlag, Berlin 2010, p. 227.

[5] A. Maziewski, J. Fassbender, J. Kisielewski, M. Kisielewski, Z. Kurant, P. Mazalski, F. Stobiecki, A. Stupakiewicz, I. Sveklo, M. Tekielak, A. Wawro, V. Zablotskii, *Phys. Status Solidi A* **211**, 1005 (2014).

[6] M. Kisielewski, A. Maziewski, M. Tekielak, J. Ferré, S. Lemerle, V. Mathet, C. Chappert, *J. Magn. Magn. Mater.* **260**, 231(2003).

[7] J. Ferré, C. Chappert, H. Bernas, J.-P. Jamet, P. Meyer, O. Kaitasov, S. Lemerle, V. Mathet, F. Rousseaux, H. Launois, *J. Magn. Magn. Mater.* **198-199**, 191 (1999).

[8] T. Devolder, J. Ferré, C. Chappert, H. Bernas, J.-P. Jamet, V. Mathet, *Phys. Rev. B* **64**, 064415 (2001).

[9] J. Ferré, T. Devolder, H. Bernas, J.-P. Jamet, V. Repain, M. Bauer, N. Vernier, C. Chappert, *J. Phys. D Appl. Phys.* **36**, 3103 (2003).

[10] N. Bergeard, J.-P. Jamet, J. Ferré, A. Mougin, B. Rodmacq, V. Baltz, J. Fassbender, *J. Appl. Phys.* **108**, 103915 (2010).

[11] H. Bernas, J.-Ph. Attané, K.-H. Heinig, D. Halley, D. Ravelosona, A. Marty, P. Auric, C. Chappert, Y. Samson, *Phys. Rev. Lett.* **91**, 077203 (2003).

[12] C.T. Rettner, S. Anders, J.E.E. Baglin, T. Thomson, B.D. Terris, *Appl. Phys. Lett.* **80**, 279 (2002).

[13] C. Vieu, J. Gierak, H. Launois, T. Aign, P. Meyer, J.-P. Jamet, J. Ferré, C. Chappert, T. Devolder, V. Mathet, H. Bernas, *J. Appl. Phys.* **91**, 3103 (2002).

[14] A. Wawro, Z. Kurant, M. Tekielak, M. Jakubowski, A. Pietruczik, R. Böttger, A. Maziewski, *Appl. Phys. Lett.* **110**, 252405 (2017).

[15] A. Wawro, Z. Kurant, M. Jakubowski, M. Tekielak, A. Pietruczik, R. Böttger, A. Maziewski, *Phys. Rev. Appl.* **9**, 014029 (2018).

[16] J. Jaworowicz, A. Maziewski, P. Mazalski, M. Kisielewski, I. Sveklo, M. Tekielak, V. Zablotskii, J. Ferré, N. Vernier, A. Mougin, A. Henschke, J. Fassbender, *Appl. Phys. Lett.* **95**, 022502 (2009).

[17] M. Sakamaki, K. Amemiya, M.O. Liedke, J. Fassbender, P. Mazalski, I. Sveklo, A. Maziewski, *Phys. Rev. B* **86**, 024418 (2012).

[18] E. Liskova, M. Veis, S. Visnovsky, J. Ferré, A. Mougin, P. Mazalski, A. Maziewski, M.O. Liedke, J. Fassbender, *Thin Solid Films* **520**, 7169 (2012).

[19] P. Mazalski, Z. Kurant, A. Maziewski, M.O. Liedke, J. Fassbender, L.T. Baczewski, A. Wawro, *J. Appl. Phys.* **113**, 17C109 (2013).

[20] M. Sakamaki, K. Amemiya, I. Sveklo, P. Mazalski, M.O. Liedke, J. Fassbender, Z. Kurant, A. Wawro, A. Maziewski, *Phys. Rev. B* **94**, 174422 (2016).

[21] E. Jakubisova-Liskova, S. Visnovsky, A. Wawro, L.T. Baczewski, P. Mazalski, A. Maziewski, M.O. Liedke, J. McCord, J. Fassbender, *J. Appl. Phys.* **115**, 17C106 (2014).

[22] A. Maziewski, P. Mazalski, Z. Kurant, M.O. Liedke, J. McCord, J. Fassbender, J. Ferré, A. Mougin, A. Wawro, L.T. Baczewski, A. Rogalev, F. Wilhelm, T. Gemming, *Phys. Rev. B* **85**, 054427 (2012).

[23] P. Mazalski, I. Sveklo, Z. Kurant, K. Ollefs, A. Rogalev, F. Wilhelm, J. Fassbender, L.T. Baczewski, A. Wawro, A. Maziewski, *J. Synchrotron Rad.* **22**, 753 (2015).

[24] K.A. Avchaciov, W. Ren, F. Djurabekova, K. Nordlund, I. Sveklo, A. Maziewski, *Phys. Rev. B* **92**, 104109 (2015).

[25] D. Weller, R.F.C. Farrow, R.F. Marks, G.R. Harp, H. Notarys, G. Gorman, *Mater. Res. Soc. Symp. Proc.* **313**, 791 (1993).

[26] J. Gierak, E. Bourhis, M.N. Merat Combes, Y. Chriqui, I. Sagnes, D. Mailly, P. Hawkes, R. Jede, L. Bruchhaus, L. Bardotti, B. Prevel, A. Hannour, P. Melinon, A. Perez, J. Ferree, J.-P. Jamet, A. Mougine, C. Chappert, V. Mathet, *Microelectron. Eng.* **78-79**, 266 (2005).

[27] B.K. Tanner, D.E. Joyce, T.P.A. Hase, I. Pape, P.J. Grundy, *Adv. X-Ray Anal.* **40**, 132 (1997).

[28] J. Gierak, D. Mailly, P. Hawkes, R. Jede, L. Bruchhaus, L. Bardotti, B. Prevel, P. Melinon, A. Perez, R. Hyndman, J.-P. Jamet, J. Ferre, A. Mougin, C. Chappert, V. Mathet, P. Warin, J. Chapman, *Appl. Phys. A* **80**, 187 (2005).

[29] R. Hyndman, P. Warin, J. Gierak, J. Ferré, J.N. Chapman, J.-P. Jamet, V. Mathet, C. Chappert, *J. Appl. Phys.* **90**, 3843 (2001).

[30] J.H. Franken, H.J.M. Swagten, B. Koopmans, *Nature Technol.* **7**, 499 (2012).

[31] J. Fassbender, J. McCord, *J. Magn. Magn. Mater.* **320**, 579 (2008).

[32] V. Mathet, T. Devolder, C. Chappert, J. Ferré, S. Lemerle, L. Belliard, G. Guentherodt, *J. Magn. Magn. Mater.* **260**, 295 (2003).

[33] J.F. Ziegler, *Handbook of Ion Implantation Technology*, North-Holland, Amsterdam 1992.

[34] Y.-T. Cheng, *Mater. Sci. Rep.* **5**, 45 (1990).

[35] J. Gierak, *Nanofabrication* **1**, 35 (2014).

[36] W. Möller, W. Eckstein, J.P. Biersack, *Comput. Phys. Commun.* **51**, 355 (1988).

[37] T. Devolder, Ph.D. Thesis, University of Paris XI, Orsay 2000.

[38] A. Berger, H. Hopster, *J. Appl. Phys.* **79**, 5619 (1996).

[39] V. Grolier, J. Ferré, A. Maziewski, E. Stefanowicz, D. Renard, *J. Appl. Phys.* **73**, 5939 (1993).

[40] A. Maziewski, V. Zablotskii, M. Kisielewski, *Phys. Status Solidi A* **189**, 1001 (2002).

[41] M. Kisielewski, A. Maziewski, T. Polyakova, V. Zablotskii, *Phys. Rev. B* **69**, 184419 (2004).

[42] A. Maziewski, J. Fassbender, J. Kisielewski, M. Kisielewski, Z. Kurant, P. Mazalski, F. Stobiecki, A. Stupakiewicz, I. Sveklo, M. Tekielak, A. Wawro, V. Zablotskii, *Phys. Status Solidi A* **211**, 1005 (2014).

[43] R.L. Novak, P.J. Metaxas, J.-P. Jamet, R. Weil, J. Ferré, A. Mougin, S. Rohart, R.L. Stamps, P.-J. Zermatten, G. Gaudin, V. Baltz, B. Rodmacq, *J. Phys. D Appl. Phys.* **48**, 235004 (2015).

[44] A. Berger, H. Hopster, *J. Appl. Phys.* **79**, 5619 (1996).

[45] T. Diaz de la Rubia, R.S. Averback, R. Benedek, W.E. King, *Phys. Rev. Lett.* **59**, 1930 (1987).

[46] R.S. Averback, *J. Nucl. Mater.* **216**, 49 (1994).

[47] S.E. Donnelly, R.C. Birtcher, *Philos. Mag. A* **79**, 133 (1999).

[48] M. Ghaly, K. Nordlund, R.S. Averback, *Philos. Mag. A* **79**, 795 (1999).

[49] M.M. Jakas, E.M. Bringa, *Phys. Rev. B* **62**, 824 (2000).

[50] F.M. Schulson, *J. Nucl. Mater.* **83**, 239 (1979).

[51] G.R. Harp, D. Weller, T.A. Rabedeau, R.F.C. Farrow, M.F. Toney, *Phys. Rev. Lett.* **71**, 2493 (1993).

[52] R.F.C. Farrow, G. Harp, D. Weller, R.F. Marks, M.F. Toney, A. Cebollada, T.A. Rabedeau, *Proc. SPIE* **2140**, 106 (1994).

[53] Y. Yamada, T. Suzuki, H. Kanazawa, J.C. Österman, *J. Appl. Phys.* **85**, 5094 (1999).

[54] Y. Yamada, W.P. Van Drent, T. Suzuki, R.N. Abarra, *J. Magn. Soc. Jpn.* **22** Suppl. N S2, 81 (1998).

[55] D. Weller, H. Brändle, C. Chappert, *J. Magn. Magn. Mater.* **121**, 461 (1993).

[56] J.O. Cross, M. Newville, B.B. Maranville, C. Bordel, F. Hellman, V.G. Harris, *J. Phys. Condens. Matter* **22**, 146002 (2010).

[57] J. Kim, J.-W. Lee, J.-R. Jeong, S.-C. Shin, Y.H. Ha, Y. Park, D.W. Moon, *Phys. Rev. B* **65**, 104428 (2002).

[58] T. Aign, P. Meyer, S. Lemerle, J.-P. Jamet, J. Ferré, V. Mathet, C. Chappert, J. Gierak, C. Vieu, F. Rousseaux, H. Launois, H. Bernas, *Phys. Rev. Lett.* **81**, 5656 (1998).

[59] P. Warin, R. Hyndman, J. Gierak, J.N. Chapman, J. Ferré, J.-P. Jamet, V. Mathet, C. Chappert, *J. Appl. Phys.* **90**, 3850 (2001).

[60] Gang Xiong, D.A. Allwood, M.D. Cooke, R.P. Cowburn, *Appl. Phys. Lett.* **79**, 3461 (2001).

[61] J.-P. Jamet, J. Ferré, P. Meyer, J. Gierak, C. Vieu, F. Rousseaux, C. Chappert, V. Mathet, *IEEE Trans. Magn.* **37**, 2120 (2001).

[62] A. Ruotolo, S. Wiebel, J.-P. Jamet, N. Vernier, D. Pullini, J. Gierak, J. Ferré, *Nanotechnology* **17**, 3308 (2006).

[63] J.-P. Adam, J.-P. Jamet, J. Ferré, A. Mougin, S. Rohart, R. Weil, E. Bourhis, J. Gierak, *Nanotechnology* **21**, 445302 (2010).

[64] J. Jaworowicz, V. Zablotskii, J.-P. Jamet, J. Ferré, N. Vernier, J.-Y. Chauleau, M. Kisielewski, I. Sveklo, A. Maziewski, J. Gierak, E. Bourhis, *J. Appl. Phys.* **109**, 093919 (2011).

[65] M. Cormier, A. Mougin, J. Ferré, J.-P. Jamet, R. Weil, J. Fassbender, V. Baltz, B. Rodmacq, *J. Phys. D Appl. Phys.* **44**, 215002 (2011).